Proceedings Paper:

Comparative Study of Axial-Flux Switched Reluctance Machine with Different Core Materials

Yangye Ji
Electronic and Electrical Engineering department
University of Sheffield
Sheffield, United Kingdom
yji22@sheffield.ac.uk

Guang-Jin Li
Electronic and Electrical Engineering department
University of Sheffield
Sheffield, United Kingdom
g.li@sheffield.ac.uk

Abstract—**This paper investigates the impact of core materials on the electromagnetic performance of 3-phase, 12-slot/8-pole axial-flux switched reluctance machines (AFSRMs) with either soft magnetic composite or laminated silicon iron on the stator/rotor teeth and stator/rotor yoke. For the investigations, the double layer mutually coupled AFSRMs supplied by sinewave current have been chosen. 2D finite-element analysis (FEA) has been adopted to evaluate the machine performance in terms of inductances, on-load torque, and losses. Furthermore, the torque-speed characteristics between different core material configurations have been compared. The comparison results have shown that the design with laminated silicon iron stator and soft magnetic composite rotor can achieve similar torque performance with the silicon iron core AFSRM at rated current. However, the soft magnetic composite rotor could significantly ease the manufacture for an axial flux design.**

Keywords—Axial-flux, mutually coupled, sine-wave current, soft magnetic composite, switched reluctance machine.

I. INTRODUCTION

WITH the development of modern power electronics, switched reluctance machines (SRMs) have regained attention from researchers with its well-known simple and robust structure. Additionally, its magnet-free feature provides possibility for operation in harsh environments and high-speed conditions [1-3]. However, although with the above advantages, the doubly salient structure with traditional square wave current supply mode often results in high torque ripple and vibrations. Authors in [4-7] proposed double layer mutually coupled (DLMC) SRMs with sinewave current supply that can achieve lower vibrations and acoustic noise compared to conventional SRMs. However, it is worth mentioning that the torque density of SRMs is not as promising as permanent magnet synchronous motors due to relatively low magnetic field intensity. To mitigate the disadvantage of SRMs in terms of relatively low torque density, axial-flux switched reluctance machine (AFSRM) has been introduced as its air-gap area is larger compared to traditional radial-flux design, leading to potentially increased torque density [8].

However, although the axial flux machines have the above advantages, their manufacturing could be more challenging than radial flux machines. In radial flux machines, laminated iron core has been the commonly used core material due to its good permeability. This technology is very mature and hence it has reasonably low cost. If the laminated iron core is to be used in an axial flux machine, the stacking direction should be perpendicular to the flux paths to reduce the iron losses, as in a radial flux machine. This will significantly increase the manufacturing complexity and hence cost. To ease the manufacturing of the axial flux machines, soft magnetic composites (SMCs) having good formability has provided a

potential alternative to the laminated steel [9]. In addition to simplifying the manufacture process, SMCs also possess various advantages against laminated iron core, such as magnetic and thermal isotropy, and lower core loss at high frequency [9-10]. Thanks to the fast evolved additive manufacturing technology that is becoming more and more mature, the 3D printed SMC has already been developed and realized in machine core making [11-12]. In [13], the selective laser melting (SLM) printing is applied not only on the core materials but also on the conductive materials such as windings. As a result, due to the separation of individual turns in the coils, the induced eddy currents can be significantly reduced.

Furthermore, the hybrid cores with the core designed as SMC in the middle and several stacks of laminated steel sheet on its surface, has also been applied to axial flux permanent magnet machines (AFPMSM) to reduce the eddy current losses [14]. This paper proposes four novel axial flux switched reluctance machines (AFSRMs) made of various core material combinations (laminated silicon iron and/or SMC) on different parts of the machine, with their electromagnetic performances compared against machines made of SMC or laminated silicon iron only.
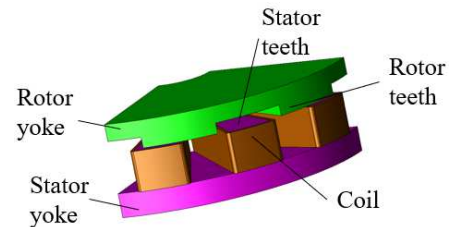
Fig. 1 3D view of the designed 12s/8p AFSRM with double layer windings.
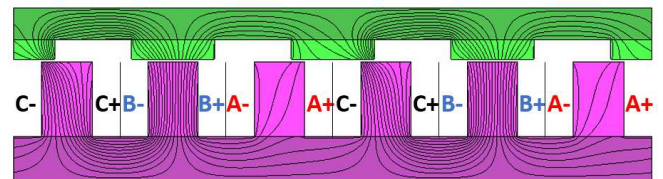
Fig. 2 Flux line distributions of the 12/8 AFSRMs with double layer mutually coupled (DLMC) winding.

TABLE I SPECIFICATIONS OF THE INVESTIGATED MACHINES

Stator/rotor outer diameter (mm)	140	Nº of turns per slot	66
Stator/rotor inner diameter (mm)	30	Rated RMS current (A)	10
Axial length (mm)	36.1	Rated speed (rpm)	400
Air gap length (mm)	0.5	Core Material	M330-35A

II. INFLUENCE OF CORE MATERIAL ON SELF- AND MUTUAL-FLUX LINKAGE

Fig. 1 provides a 3D overview of the investigated 12s/8p AFSRM. Fig. 2 shows the DLMC winding configuration and the 2D flux line distribution at aligned position with phase A supplied with a DC current. Key design parameters are given in TABLE I. The dimensions of the AFSRMs, such as stator/rotor pole width, split ratio, stator/rotor yoke thickness, etc., have been fully optimized. It is worth noting that the original machine for the optimization has used laminated silicon iron core. The six representative core material combinations are given in TABLE II. Meanwhile, typical type of materials have been chosen as representatives for the SMC and silicon iron, i.e., Somaloy 700 3P and M330-35A, respectively. Their magnetization curves are given in Fig. 3, showing that the silicon iron possesses higher flux density than the SMC, but it is easier to be saturated, leading to potentially limited overload capability.

TABLE II CORE MATERIAL COMBINATIONS OF THE INVESTIGATED MACHINES

	Stator		Rotor	
	Yoke	Teeth	Yoke	Teeth
Design 1	**SMC**	**SMC**	**SMC**	**SMC**
Design 2	SMC	Silicon iron	SMC	Silicon iron
Design 3	Silicon iron	SMC	Silicon iron	SMC
Design 4	**Silicon iron**	**Silicon iron**	**Silicon iron**	**Silicon iron**
Design 5	Silicon iron	Silicon iron	SMC	SMC
Design 6	SMC	SMC	Silicon iron	Silicon iron
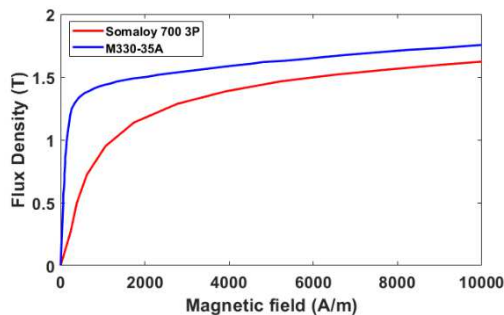
Fig. 3 Magnetization curves of typical SMC and silicon iron materials.

It is worth noting that both the direct 3D FE and equivalent 2D FE modelling have been carried out for the investigations in this paper, they have shown a good match. Therefore, to reduce the computation time, only 2D FE results have been presented in the following sections. By using the 2D FE modelling, the self and mutual flux linkages of the DLMC-AFSRMs have been calculated first (see Fig. 4), as they can be used to predict the torque generation capability of SRMs. By observing the co-energy, which is the area enclosed by the loci of flux linkage between aligned and unaligned positions, torque produced by each material combination can be estimated. The relationship between co-energy and torque can be expressed by

$$T = \frac{\partial W'(i,\theta)}{\partial \theta}\bigg|_{i=constant} \quad \text{and} \quad T_{av} = \frac{mp}{2\pi} \times W' \qquad (1)$$

where T is the instantaneous torque, T_{av} is the average torque, W' is the co-energy, i is the instantaneous phase current, θ is

the rotor position, m is the number of phases, and p is the number of pole pairs.
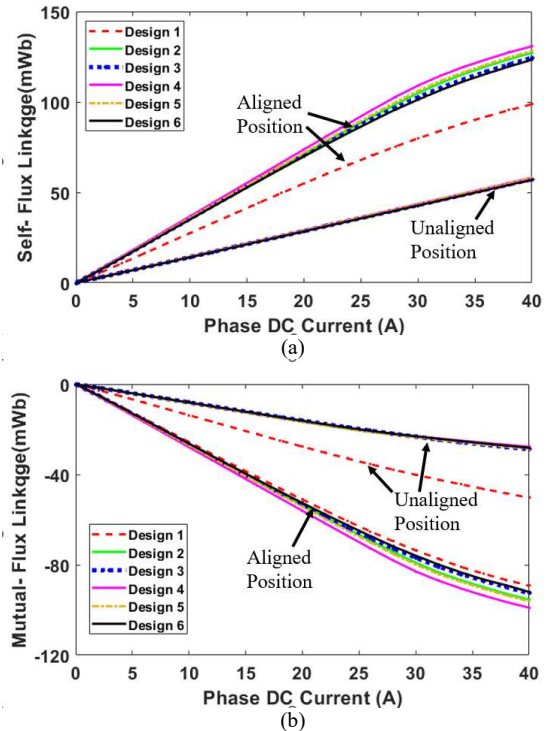
Fig. 4 Comparison of (a) self flux-linkage and (b) mutual flux-linkage at aligned and unaligned positions.

Fig. 4 shows the self and mutual flux-linkages at aligned and unaligned positions of the six core material combinations. The area enclosed by the aligned and unaligned self flux-linkage of Design 4 is significantly larger than Design 1 [see Fig. 4 (a)], leading to a great difference on their self-torque capability. Besides, the hybrid core designs have similar self-coenergy level as the laminated silicon iron core machine, following an order such as Design 5 > Design 2 > Design 3 > Design 6. Similar conclusion can be drawn from Fig. 4 (b) for the mutual flux-linkages. It is worth mentioning that the self flux-linkages of the six material combinations at unaligned position are almost identical, whilst the pure SMC core machine has a non-negligible difference in unaligned mutual flux-linkage [see Fig. 4 (b)]. In terms of the core saturation, the flux-linkages of Design 3 and Design 6 have an almost linear rise when current increases, and hence have the best performance amongst all the four hybrid core machines.

III. ONLOAD STATIC PERFORMANCE ANALYSIS

To reveal the influence of magnetic saturation on the torque performance, various level (from 10 A_{rms} to 40 A_{rms}) of sinewave current has been supplied to the investigated AFSRMs. Average torque has been compared first, as shown in Fig. 5 and TABLE IV in the Appendix. At current level lower than 25 A_{rms}, as expected, the average torque of Design 4 (pure silicon iron core) rises linearly with current, and it is the highest amongst all the six designs. Once the current threshold has been exceeded, the Design 4 starts to saturate, resulting in relatively flattened torque-current curve at high current level [see Fig. 5 (a)]. On the contrary, Design 1 has a linear torque performance when current level increases, resulting in 10.6% lower average torque at the rated current but 2.2% higher torque at 40 A_{rms} compared to Design 4. In the

meantime, Design 5 has the highest torque amongst the four hybrid core machines at the rated current (1.81 Nm), but still 4.2% lower than Design 4. On the other hand, Design 6 provides the optimal torque at 40 A_{rms}, 5.2% higher than Design 4. In terms of the torque ripple, as can be seen from TABLE IV and Fig. 5 (b), same as the average torque, Design 4 provides the most preferable results from 0 to 30 A_{rms}, with Design 6 becoming the best after 30 A_{rms}. Meanwhile, the torque ripple coefficients of the six designs at the rated condition are very much similar, with only 3% difference between the best and poorest designs. Based on the findings from the torque-current curves and torque ripple-current curves, Design 5 can be regarded as the best alternative to the pure silicone iron core design at rated condition.

(a)

(b)
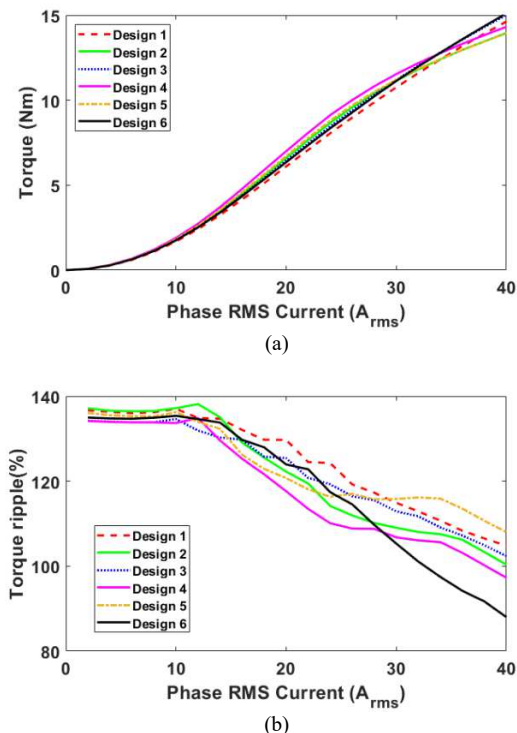
Fig. 5 Performance comparisons at different current level. (a) average torque, (b) torque ripple rate.

In addition to the torque performance, the various core material combinations will also have different influences on the iron core losses. Comparisons of the iron loss against phase RMS currents and rotor speeds are shown in Fig. 6. As expected, under low frequency operation, Design 4 (pure silicon iron core) produces the lowest iron core losses and Design 1 (pure SMC core) produces the highest iron core losses amongst the six designs, with Design 5 once again achieving a performance closest to the Design 4 at different currents [see Fig. 6 (a)]. At the rated current and the rated speed condition, though the iron loss of Design 5 (1.61 W) is 40% higher than Design 4 (1.15 W), the levels of iron losses in all the designs are insignificant compared to the copper losses in these relatively small machines. On the other hand, Fig. 6 (b) shows that the relationships of total iron loss levels between different core materials vary significantly with rotor speed. It can be observed that the iron loss of Design 1 becomes competitive against Design 4 after the speed reaches 10000 rpm. As mentioned before, SMC possesses high resistivity that leads to low eddy current loss [see Fig. 6 (c)].

Though the porous microstructure of SMC causes highest hysteresis loss amongst the six designs [see Fig. 6 (d)], the eddy current loss dominates the total iron loss at high-speed condition, leading to a more desirable iron loss performance compared to the pure silicon iron core machine. Similarly, Design 5 produces the lowest total iron loss from 5000 rpm to 15000 rpm.

(a)

(b)

(c)

(d)
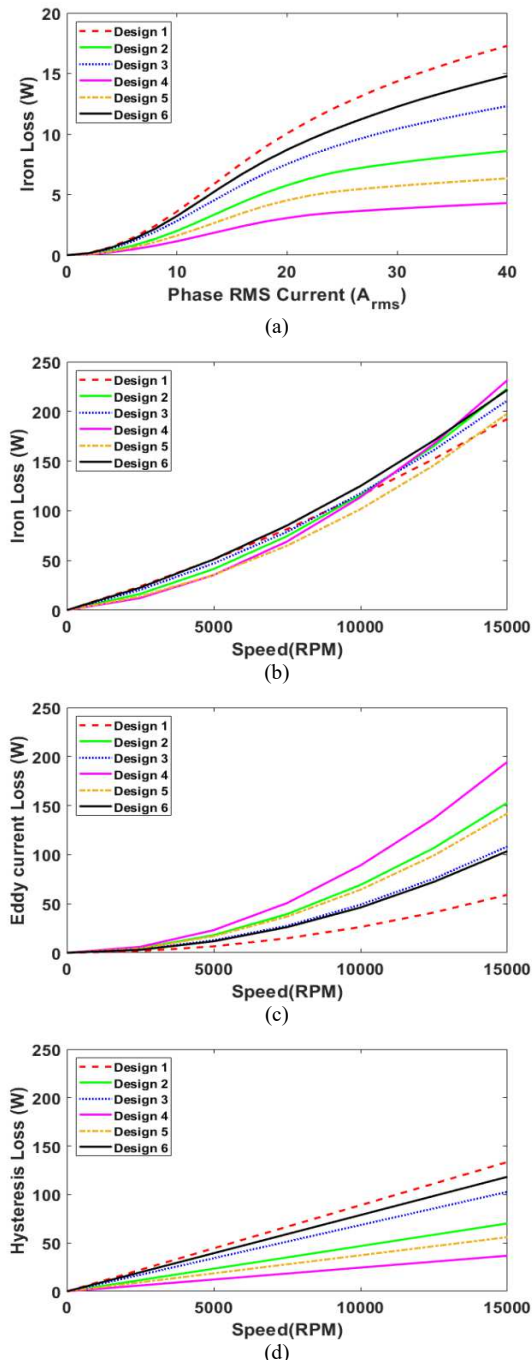
Fig. 6 Comparison of iron losses amongst different designs. (a) total iron losses at rated speed with increasing phase RMS current, (b) total iron losses at rated current with increasing rotor speed, (c) eddy current losses at rated current with increasing rotor speed, and (d) hysteresis losses at rated current with increasing rotor speed.

IV. DYNAMIC PERFORMANCE ANALYSIS

In the previous section, the onload torques at a fixed speed and current have been investigated. As aforementioned, machines with different core material combinations result in diverse characteristics of their self- and mutual inductances

and hence will also have an impact on the machine dynamic performance. In this section, further analyses on the torque-speed characteristics, iron losses and efficiency maps have been carried out.

A. Torque Speed Curves

The torque-speed curve analyses are based on (2) in abc-reference frame. The self- and mutual inductances have been calculated using 2D FE models.

$$T_e(i,\theta) = \frac{1}{2}i_a^2\frac{dL_a}{d\theta} + \frac{1}{2}i_b^2\frac{dL_b}{d\theta} + \frac{1}{2}i_c^2\frac{dL_c}{d\theta} + i_ai_b\frac{dM_{ab}}{d\theta}$$
$$+ i_ai_c\frac{dM_{ac}}{d\theta} + i_bi_c\frac{dM_{bc}}{d\theta}$$

(2)

where i_a, i_b, i_c, L_a, L_b, L_c, M_{ab}, M_{bc} and M_{ac} are 3-phase currents, self- and mutual inductances, respectively, whilst θ is the rotor mechanical position.
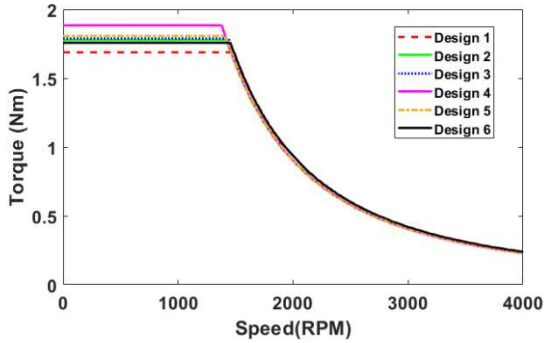
Fig. 7 Torque-speed characteristics of the 6 designed AFSRMs.

TABLE III BASE SPEED OF THE 6 INVESTIGATED MACHINES

Winding Configuration	Base speed
Design 1	1480 rpm
Design 2	1420 rpm
Design 3	1440 rpm
Design 4	1380 rpm
Design 5	1410 rpm
Design 6	1450 rpm

Fig. 7 compares the torque-speed curves of the six investigated machines, with TABLE III specifying their base speeds. It is known already from the previous sections that Design 4 has the highest average torque, whilst Design 1 has the lowest. On the contrary, the base speeds of the six designs at rated condition from high to low follows exactly the opposite order with average torque discussed in part III, i.e., Design 1 > Design 6 > Design 3 > Design 2 > Design 5 > Design 4. It is worth noting that, beyond the base speeds, the dynamic performances of the six designs are almost identical. Overall, the core materials seem to have negligible impact on the base speeds and high-speed torque performances of the investigated AFSRMs.

B. Iron Losses

With the same winding configuration, the phase resistances of the six machines are identical even with consideration of the end-winding. Additionally, the current supply methods are identical as well. Therefore, the difference in copper losses for different machines would be too small for comparison study. In this case, the main focus of the losses has been put on the iron losses.

Various iron loss models have been provided in [6][15][16], for simplicity, in this paper, the lookup table method has been adopted with (3) generally illustrating the basic principle for calculating the iron losses at different rotor speeds.

$$\begin{cases} P_{eddy}(\omega) = k_{eddy} \cdot (fB)^2 \\ P_{hys}(\omega) = k_{hys} \cdot f^\alpha B^\beta \end{cases}$$

(3)

where P_{eddy}, P_{hys}, k_{eddy}, k_{hys}, f, and B are eddy-current loss, hysteresis loss, eddy current coefficient, hysteresis coefficient, frequency, and flux density, respectively. α and β are empiric coefficients, which vary for different core materials. In this paper, α has taken the value of 1, and β is selected by the FEA for SMC and M330-35A.

Iron loss maps have been compared amongst all the hybrid core combinations, as shown in Fig. 8. It can be clearly observed that within the speed range, i.e., 0 to 5000 rpm, the highest iron loss amongst all the designs is 12 W. All designs reached their highest iron loss level at base speed while the maximum torque is achieved. This is because of the application of high current and relatively high speed. Design-5 (rotor SMC and stator laminated steel) has been found to be the most desirable design, with a close level of iron loss compared to the pure silicon iron at low speed. On the contrary, Design 1 and Design 6 with relatively more SMC used in the machine, have the highest peak iron loss level at their maximum-torque around the base speed region.

(a)

(b)

(c)

(d)

(e)

(f)
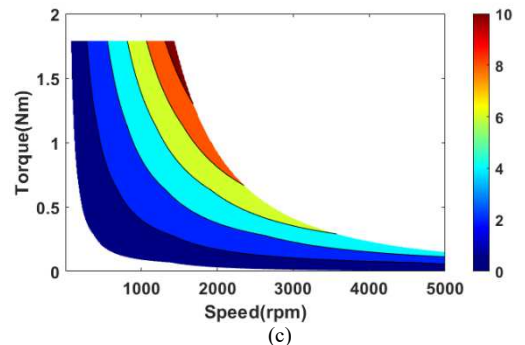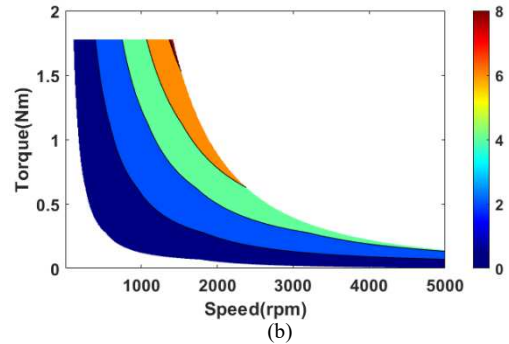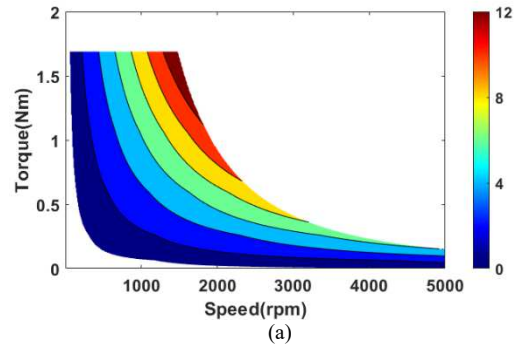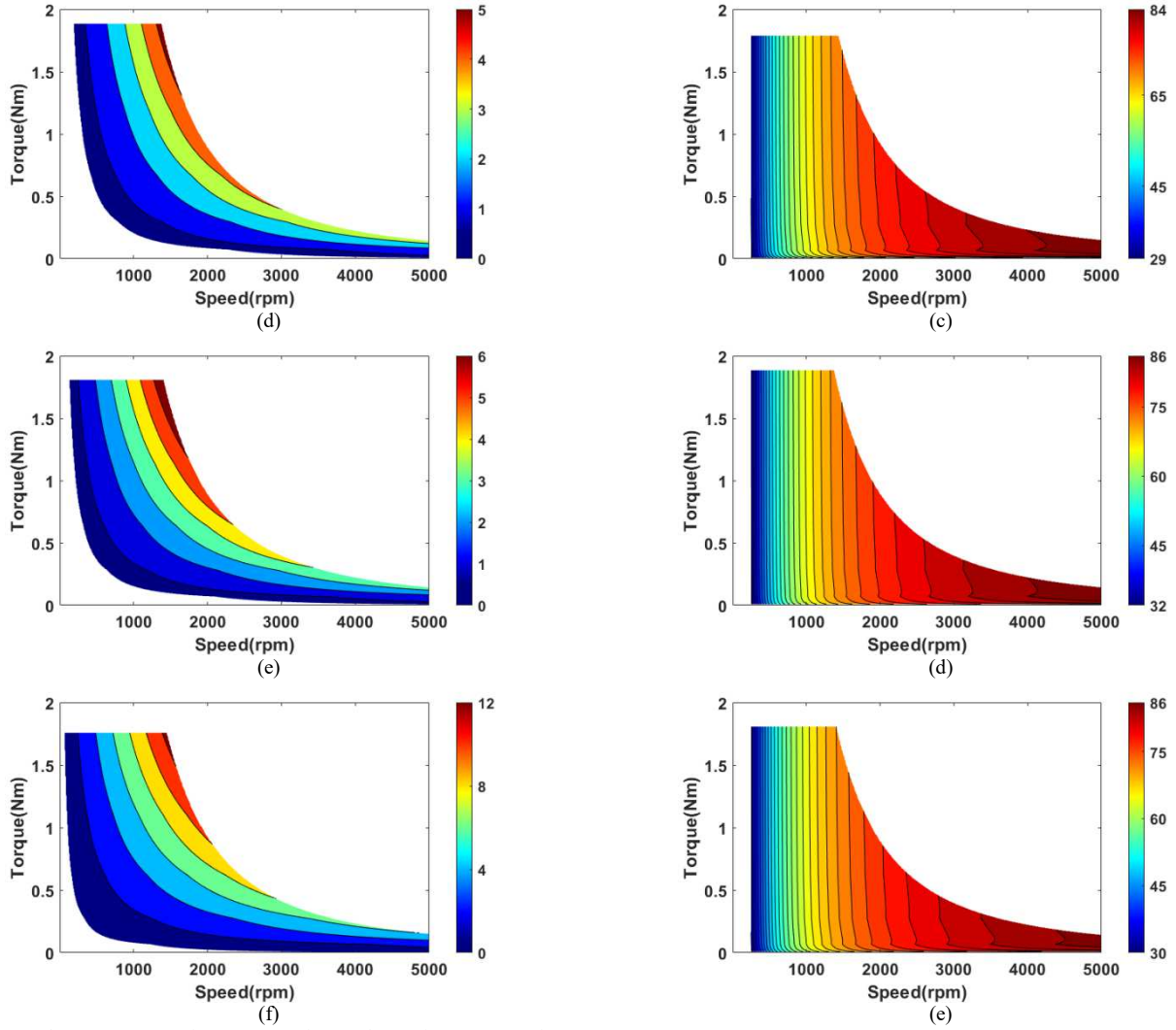
Fig. 8 Iron loss map comparisons. (a) Design 1, (b) Design 2, (c) Design 3, (d) Design 4, (e) Design 5, and (f) Design 6.

(a)

(b)

(c)

(d)

(e)

(f)
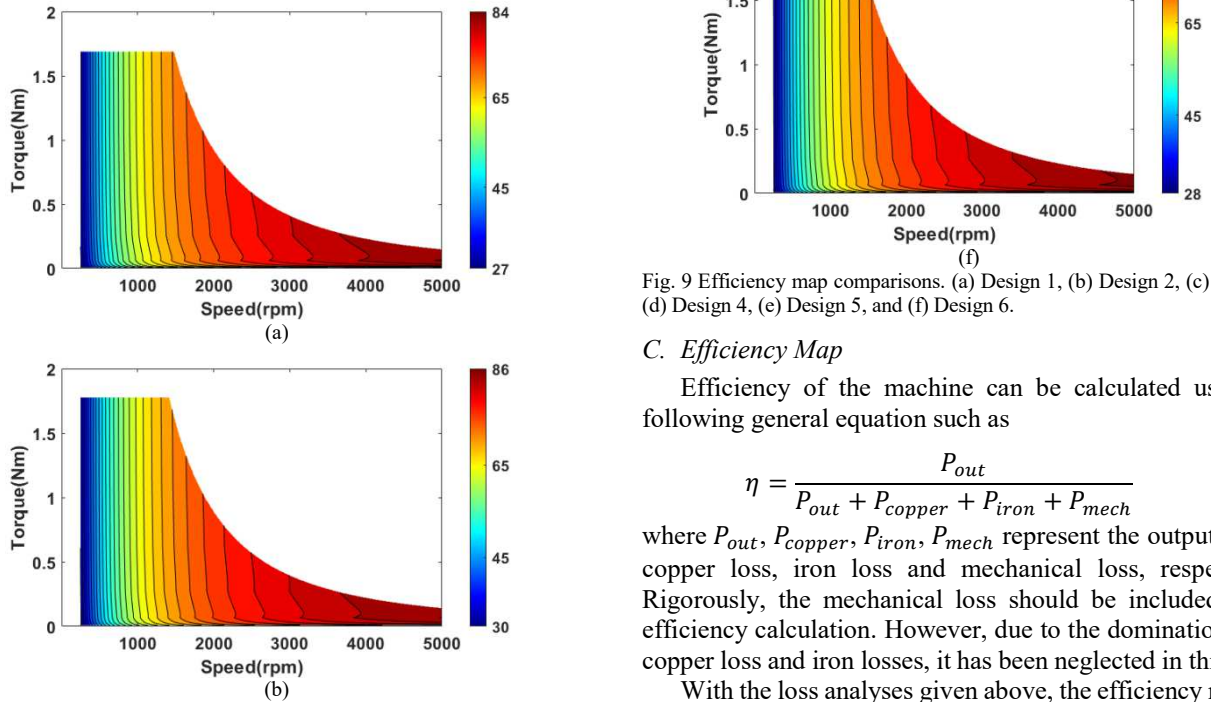
Fig. 9 Efficiency map comparisons. (a) Design 1, (b) Design 2, (c) Design 3, (d) Design 4, (e) Design 5, and (f) Design 6.

C. Efficiency Map

Efficiency of the machine can be calculated using the following general equation such as

$$\eta = \frac{P_{out}}{P_{out} + P_{copper} + P_{iron} + P_{mech}} \quad (4)$$

where P_{out}, P_{copper}, P_{iron}, P_{mech} represent the output power, copper loss, iron loss and mechanical loss, respectively. Rigorously, the mechanical loss should be included in the efficiency calculation. However, due to the domination of the copper loss and iron losses, it has been neglected in this study.

With the loss analyses given above, the efficiency map can provide a more straightforward view about the optimal

operating range of the machines. As can be seen from Fig. 9, the efficiency of the sinewave current supplied AFSRM increases with speed, up to 86%. This is due to the domination of the iron losses compared to the copper loss at high speed operation zone. Additionally, as mentioned in section III, the iron losses started to have observably exponential growth only after 10000 rpm. Here, the speed range chosen based on the torque speed curve is limited to 5000 rpm. Therefore, a more obvious different in efficiency has not yet shown up in this speed range. As a result, it is worth noting that the differences between the different material combinations is negligible, with only ±5% variation on the efficiency range. Surprisingly, the pure SMC core machine can reach up to 84% efficiency within the speed range, but with lower average torque. On the other hand, as expected, the pure silicon iron core machine gives the best performance. However, Design-5 again achieves the closest dynamic performance to the pure silicon iron core design.

V. CONCLUSION

This paper investigates the 12-slot/8-pole axial-flux switched reluctance machines with various core material combinations. The analyses are based on 2D FEA. Six core designs, pure SMC core, yoke (SMC) with teeth (silicon iron), yoke (silicon iron) with teeth (SMC), pure silicon iron core, rotor (SMC) with stator (silicon iron), and rotor (silicon iron) with stator (SMC) have been employed for the comparative study. With the sinewave current supplied, the influences of the core materials on average torque, torque ripple, iron core losses, torque-speed characteristics and efficiency map have been investigated. Differences between designs were more obvious for the static performances rather than for the dynamic performances. This is mainly because the core losses only exhibit significant differences at much higher rotor speeds, thereby resulting in minor variations in efficiency within the chosen speed range in this paper. Amongst all the designs, the pure silicon iron core design has the highest torque capability and the lowest torque ripple coefficient (134%) at low speed. The rotor (SMC) with stator (silicon iron) design can achieve similar performance with only 4.2% reduced average torque compared to the pure silicon iron core design, but with much simplified machine manufacture process and reduced cost, and hence provides a viable alternative to the pure silicon iron core axial flux machine.

REFERENCES

[1] T. J. E. Miller, "Optimal design of switched reluctance motors," *IEEE Trans. Ind. Electron.*, vol. 49, no. 1, pp. 15-27, Feb. 2002.
[2] G. J. Li, J. Ojeda, E. Hoang, M. Lecrivain, and M. Gabsi, "Comparative studies between classical and mutually coupled switched reluctance motors using thermal-electromagnetic analysis for driving cycles," *IEEE Trans. Magn.*, vol. 47, no. 4, pp. 839-847, Apr. 2011.
[3] W. Hua, H. hua, N. Dai, G. Zhao, and M. Cheng, "Comparative study of switched reluctance machines with half-and full-teeth-wound windings," *IEEE Trans. Ind. Electron.*, vol. 63, no. 3, pp. 1414-1424, March 2016.
[4] G. J. Li, X. Ojeda, S. Hlioui1, E. Hoang, M. Gabsi, and C. Balpe, "Comparative study of switched reluctance motors performances for two current distributions and excitation modes," *In Proc. IEEE Ind. Electron. Conf. (IECON'09), Porto, Portugal,* Nov. 2009.
[5] X. B. Liang, G. J. Li, J. Ojeda, M. Gabsi, and Z. X. Ren, "Comparative study of classical and mutually coupled switched reluctance motors using multiphysics finite-element modeling," *IEEE Trans. Ind. Electron.*, vol. 61, no. 9, pp. 5066-5074, Sep. 2014.
[6] X. Y. Ma, G. J. Li, G. W. Jewell, Z. Q. Zhu, and H. L. Zhan, "Performance comparison of doubly salient reluctance machine topologies supplied by sinewave currents," *IEEE Trans. Ind. Electron.*, vol. 63, no. 7, pp. 4086 - 4096, Jul. 2016.
[7] G. J. Li, Z. Q. Zhu, X. Y. Ma, and G. W. Jewell, "Comparative study of torque production in conventional and mutually coupled SRMs using frozen permeability," *IEEE Trans. Magn.*, vol. 52, no. 6, Jun. 2016.
[8] H. Arihara and K. Akatsu, "Basic properties of an axial-type switched reluctance motor," in *IEEE Trans. Ind. Appl.*, vol. 49, no. 1, pp. 59-65, Jan.-Feb. 2013.
[9] H. Shokrollahi.and K. Janghorban, "Soft magnetic composite materials (SMCs), " *Journal of Materials Processing Technology*, 189(1), pp. 1–12, Feb. 2007.
[10] A. Schoppa and P. Delarbre, "Soft magnetic powder composites and potential applications in modern electric machines and devices," in *IEEE Trans. Magn.*, vol. 50, no. 4, pp. 1-4, April 2014.
[11] H. -J. Pyo, J. W. Jeong, J. Yu, S. G. Lee and W. -H. Kim, "Design of 3D-printed hybrid axial-flux motor using 3D-printed SMC core," in *IEEE Trans. Appl. Supercond.*, vol. 30, no. 4, pp. 1-4, June 2020.
[12] H. Tiismus, A. Kallaste, T. Vaimann, A. Rassõlkin and A. Belahcen, "Additive manufacturing of prototype axial flux switched reluctance electrical machine," *2021 28th International Workshop on Electric Drives: Improving Reliability of Electric Drives (IWED)*, Moscow, Russia, 2021, pp. 1-4.
[13] H. Tiismus, A. Kallaste, A. Belahcen, T. Vaimann, A. Rassõlkin, and D. Lukichev, "Hysteresis measurements and numerical losses segregation of additively manufactured silicon steel for 3D printing electrical machines," *Appl. Sci.*, vol. 10, no. 18, p. 6515, 2020.
[14] B. Scheerlinck, H. De Gersem and P. Sergeant, "3-D eddy current and fringing-flux distribution in an axial-flux permanent-magnet synchronous machine with stator in laminated iron or SMC," in *IEEE Trans. Magn.*, vol. 51, no. 11, pp. 1-4, Nov. 2015.
[15] L. Ge, B. Burkhart and R. W. De Doncker, "Fast iron loss and thermal prediction method for power density and efficiency improvement in switched reluctance machines," in *IEEE Trans. Ind. Electron.*, vol. 67, no. 6, pp. 4463-4473, June 2020.
[16] S. Ferrari, P. Ragazzo, G. Dilevrano and G. Pellegrino, "Flux and loss map based evaluation of the efficiency map of synchronous machines," *IEEE Trans. Ind. Appl.*, vol. 59, no. 2, pp. 1500-1509, March-April 2023.

APPENDIX

TABLE IV AVERAGE TORQUE (NM) AND TORQUE RIPPLE COEFFICIENT (%) COMPARISON AT DIFFERENT CURRENT LEVELS

Current	Design 1	Design 2	Design 3	Design 4	Design 5	Design 6
10 A_{rms}	1.69Nm, 137%	1.78Nm, 137%	1.78Nm, 135%	1.89Nm, 134%	1.81Nm, 136%	1.75Nm, 135%
20 A_{rms}	6.10Nm, 130%	6.60Nm, 122%	6.44Nm, 125%	6.99Nm, 118%	6.72Nm, 121%	6.35Nm, 124%
30 A_{rms}	10.76Nm, 115%	11.14Nm, 109%	11.19Nm, 113%	11.53Nm, 107%	11.20Nm, 116%	11.13Nm, 105%
40 A_{rms}	14.63Nm, 105%	13.95Nm, 100%	15.02Nm, 102%	14.31Nm, 97%	13.94Nm, 108%	15.10Nm, 88%